JOURNAL OF GEOPHYSICAL RESEARCH, VOL. 102, NO. B3, PAGES 5455–5472, MARCH 10, 1997

P wave velocity tomography of the Venezuelan region from local arrival times

Miguel Bosch[1]

Departamento de Física Aplicada, Universidad Central de Venezuela, Caracas

Abstract. Arrival times from the local seismological network of Venezuela were used to estimate a three-dimensional *P* wave velocity model for the region between longitude 60°-74° W and latitude 6°-14° N to a depth of more than 80 km. The inversion was carried out by damped least squares, describing the media by homogeneous velocity blocks. The resolved lateral velocity variations in the first layer (0-30 km depth) showed a correlation with the main stratigraphic features of the area, while second layer (30-50 km depth) showed the influence of Moho depth variations through the region, generating a pattern well correlated to the Bouguer Anomaly Map. Lithospheric seismic velocities below the Moho appear to be influenced by the major crustal fault systems. An important low-velocity zone is present below the triple junction of the fault systems of Oca, Boconó, and Morón in northwestern Venezuela. Farther south, a similar low-velocity zone is present below the junction of the Boconó and the Santa Marta fault systems. Those are the two continental corners of the triangular Maracaibo Block. Below 80 km depth (the fourth layer) the low velocity zones show a connected pattern that follows or is adjacent to the crustal fault zones. The presence of subducted Atlantic lithosphere below the Eastern Venezuelan Basin could explain the high-velocity zone at this location. A similar interpretation emerges from the tectonic wedging model, previously proposed to explain the pronounced minimum of the gravity anomaly.

Introduction

The northern boundary of the South American plate is a geologically interesting area were several microplates accommodate the relative movement between major plates. The boundary between the Caribbean and the South American plates was characterized by *Jordan* [1975] as a complex and wide deformation zone [see also *Ladd et al.*, 1990]. It is formed of accreted terranes, originating in the collision of a Caribbean paleoisland arc with the South American continent [*Pindell et al.*, 1988; *Ross and Scotese*, 1988]. Present-day relative movement between the two plates is accommodated by the Maracaibo Block [*Kellogg and Bonini*, 1982], the Bonaire Block [*Silver et al.*, 1975; *Bosch and Rodríguez*, 1992], and southward by the Andean Block [*Pennington*, 1981]. In the northeast of the region, near the southward limit of the Lesser Antilles subduction zone, the process of obduction of the Caribbean Plate over the continent is still in progress [*Speed*, 1985]. The major fault systems of the area are shown in Figure 1.

Despite major research efforts the structure of the Caribbean-South American plate boundary zone is not completely clear. Global plate motion models do not produce adequate resolution of the Caribbean-South American motion [*Stein et al.*, 1988; *DeMets et al.*, 1990] because they are unable to incorporate microplate kinematics into the boundary zone. Debate is going on about the tectonics of the eastern area. There, the Caribbean plate is subducting oceanic lithosphere having oblique collision with the continental lithosphere [*Russo and Speed*, 1992]. The largest negative continental gravity anomaly is observed in eastern Venezuela. Several additional controversial subjects concern the geodynamics of the complex area under consideration.

The geophysical information used for the analysis of the structure and geodynamics of the area has been fault displacements, seismotectonic data, plate velocity estimates, gravimetric data, and shallow seismic reflection data. The objective of this work is to extract information from reported arrival times of local earthquakes to the Venezuelan seismological network to produce a *P* wave velocity tomographic image of the Venezuelan lithosphere. The breadth of the Venezuelan seismological network (Figure 2), the distribution of the seismic zone, and the depth of the earthquakes and refraction paths allowed the lithosphere to be targeted with a spatial resolution of the order of a degree below an area centered at the Boconó-Morón-El Pilar fault system [*Schubert*, 1982, 1984; *Schubert and Krause*, 1984] and the southern-

[1]Temporarily at Laboratoire de Tomografie Geophysique, Département de Sismologie, Institut de Physique du Globe de Paris.

Paper number 96JB03172.
0148-0227/97/96JB-03172$09.00

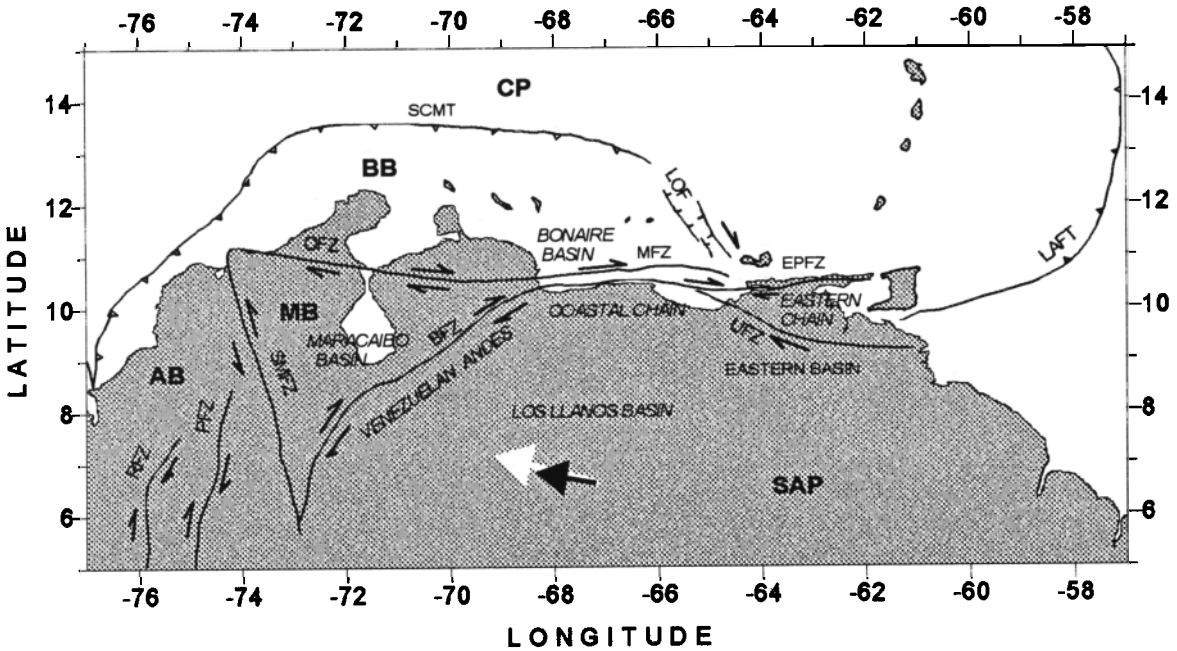

Figure 1. Major fault systems and names of structural features of the southern Caribbean-northern South America region, modified from *Mann et al.* [1990]. Bold codes are as follows: CP, Caribbean plate; SAP, South American plate; BB, Bonaire Block; MB, Maracaibo Block; and AB, Andean Block. Codes for the fault systems are as follows: BFZ, Boconó Fault Zone; MFZ, Morón Fault Zone; SMFZ, Santa Marta Fault Zone; OFZ, Oca Fault Zone; SCMT, South Caribbean Marginal Thrust; UFZ, Urica Fault Zone; EPFZ, El Pilar Fault Zone; LAFT, Lesser Antilles Fore-arc Thrust; PFZ, Palestina Fault Zone; RFZ, Romeral Fault Zone; and LOF, La Orchila Fault Zone. Vectors show the movement of the South American plate relative to the Caribbean plate. The white vector, of magnitude 22 mm/yr, is obtained from the global plate motion model RM2 [*Minster and Jordan*, 1978], and the black vector, of magnitude 13 mm/yr, is from the NUVEL-1 global model [*DeMets et al.*, 1990].

most border of the Antilles subduction zone [*Perez and Aggarwal*, 1981].

Because of the spatial resolution and the moderate size of the study area, the tomographic problem was treated by solving the normal damped least squares equations [*Aki and Lee*, 1976]. This method produces a better qualified solution than the row-action methods [*Censor*, 1981] such as ART (algebraic reconstruction technique) or SIRT (simultaneous iterative reconstruction technique) or the iterative matrix solvers [*Nolet*, 1993] such as LSQR, needed in large tomographic problems.

In the mantle, temperature seems to be the physical parameter with major influence on lateral variations of the seismic velocities. Low-velocity zones will correspond to high-temperature zones, as the two variables are anticorrelated in laboratory measurements [*Kumazawa and Anderson*, 1969; *Christensen*, 1979]. For the convecting mantle the association of lateral velocity variations with major geodynamic features has been well identified. Tomographic images show low-velocity zones for ocean ridges and high-velocity zones for subducted slabs [*Woodhouse and Dziewonski*, 1984; *Ritzwoller and Lavely*, 1995]. On a global scale, lithospheric divergence can be associated with higher mantle temperatures and lower velocities, and lithospheric convergence can be associated with lower temperatures and higher velocities [*Ricard and Vigny*, 1989; *Forte et al.*, 1993]. However, the relation between lateral velocity variations and geodynamic phenomena in the subcrustal lithosphere has not been clearly established. In this work it is hypothesized that microplate kinematics should modify conditions in the subcrustal lithosphere, particularly in microplate boundaries, producing significant velocity lateral variations. This idea is contrasted with indirect observations, coming from the P wave velocity image, examining the association of the velocity pattern with the geometry of the major fault systems of the area.

Data and Methods

The Venezuelan seismological network (Red Sismológica Venezolana de Apertura Continental) records seismic signals from 22 regular stations and reports arrival times from additional 24 seismic stations which include stations from the Universidad de los Andes network (southwest area), Trinidad network (northeast area), state electric company network (southeast area), and some sites where stations have been placed for short periods. The network maintains observation over the seismic activity of the northern South American continent and contributes to the International Seismological Center with teleseismic arrivals.

More than 700 events were reported by the network be-

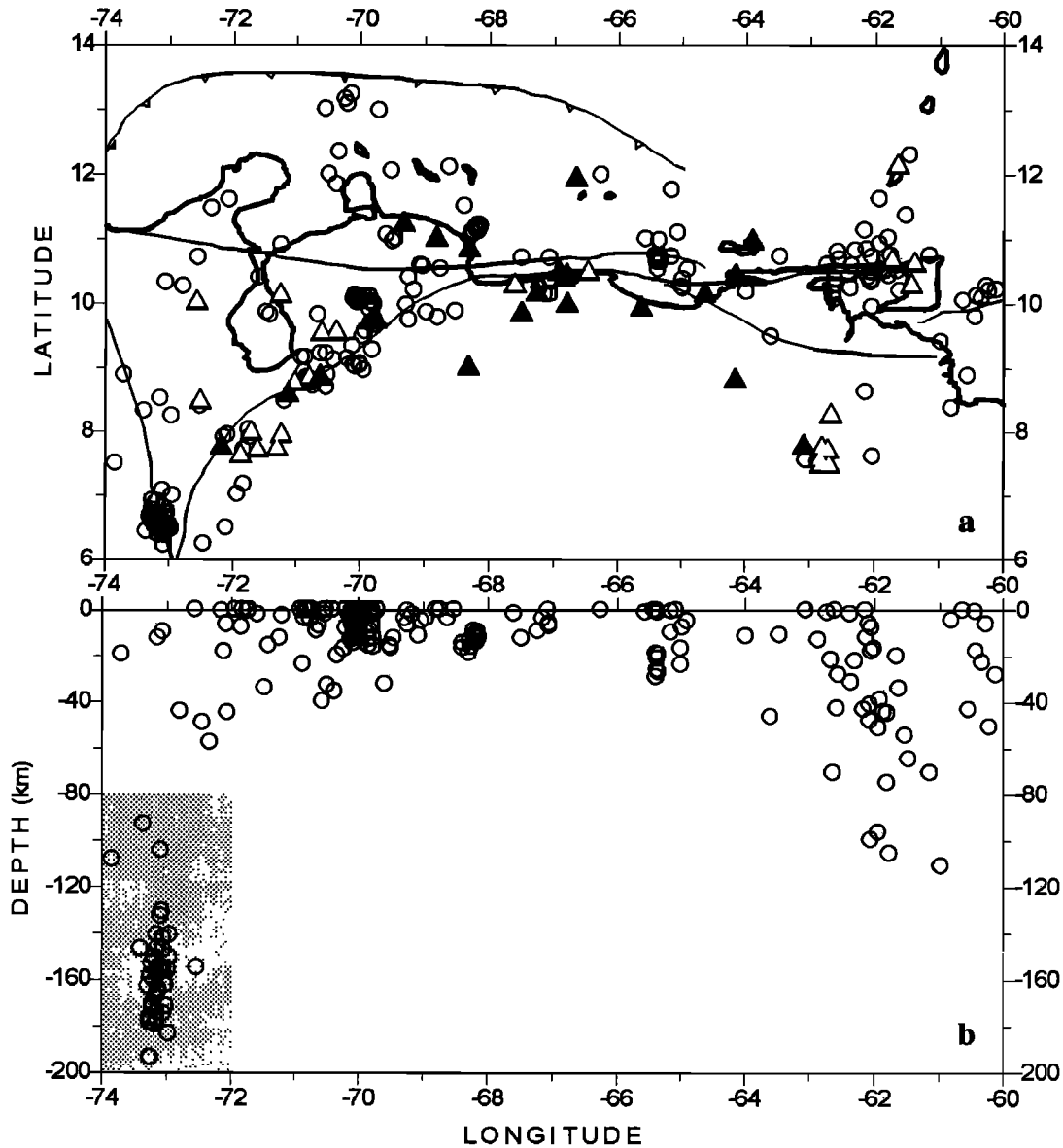

Figure 2. Map of the study region showing the seismological stations and the foci (open circles) of the 215 earthquakes used in the inversion. (a) Black triangles correspond to the 22 regular stations, and open triangles correspond to another 24 additional stations reported by the network. Lines correspond to the relevant fault systems and to the coastline (bold). (b) The projection of all foci in a vertical plane of constant latitude. The small cluster at the southwest corresponds to the Bucaramanga nest.

tween the years 1988 and 1992 [*Boletín Sismológico de Venezuela*, 1988-1992]. They were selected to form the database for the three-dimensional (3-D) inversion following a procedure based on the number of stations recording the event: (1) first arrival times should be recorded by eight or more stations, and (2) reported locations should be between longitude 60°-74° W and latitude 6°-14° N. These criteria resulted in a data set of 218 earthquakes. Arrival times for these quakes were modeled and three quakes with abnormaly large residuals were eliminated, giving a final data set of 215 earthquakes providing 2058 arrival times to the inversion. The spatial distribution of quakes and stations is shown in Figure 2. For the one-dimensional (1-D) inversion a smaller data subset of 1008 travel times was used, derived from the 104 quakes recorded by nine or more stations between the years 1988 and 1990.

Arrival times at the additional stations of the network represent only 5% of data. Arrival times to the closest of these stations are sometimes reported and used to better constrain the source location. Inversion was performed with and without additional stations to analize the influence of this data subset over the inverted 3-D velocity structure. The resulting velocity images showed significant diferences only in the northeastern and northwestern extremes of the uppermost layer, where no regular stations are placed. Because of this fact and because this data subset helps to constrain some earth-

quake locations, the additional stations were maintained in the inversion data set.

Standard deviations of the source locations, coming from the variance calculation of the 1-D inversion, have been previously used as criteria to constrain the data set for seismic local tomography. Data sets successfully used for 3-D velocity estimation were characterized by standard deviation upper bounds of 10 km in location coordinates and 1 s in origin time [*Ishida and Hasemi*, 1988; *Roecker*, 1982; *Horie and Aki*, 1982] in areas of comparable size to the one considered here. Source dispersion, independently calculated by the Venezuelan seismological network [*Boletín Sismológico de Venezuela*, 1988-1992] and by the 1-D inversion in this work, easily fits below those bounds. Moreover, after the 3-D inversion, errors in localization calculated from the variance-covariance matrix showed standard deviations below 3 km, 3 km, 6 km, and 0.5 s for coordinates x (longitude), y (latitude), z (depth), and t (origin time) with average values of 1.5 km, 2.1 km, 3.4 km, and 0.2 s, correspondingly. This dispersion is several orders of magnitude smaller than path lengths and travel times in the area and more than one order of magnitude smaller than the size of the blocks and velocity structures targeted in the inversion.

Another criteria previously used to select data sets for local seismic tomography in areas of similar size to the one under consideration is the magnitude of the residuals. *Hirahara* [1981] and *Hirahara et al.* [1989] fixed an upper bound of 5.0 s to arrival time 1-D residuals to select earthquake databases used in the two referenced tomographic studies. These studies allowed the identification of interesting features of the crust and the lithosphere in the Japan area. The arrival time 1-D residuals for the data set used here fit easily a similar requirement having absolute values below the 2.0 s. Another item for comparison between the present work and the five last referenced works is the size of the data set, ranging from 835 [*Ishida and Hasemi*, 1988] to 8800 [*Roecker*, 1982] arrival times, and the size of blocks representing the media ranging from 1° x 1° to 0.25° x 0.25°.

The earth model was described by layers, and each layer was divided into regular blocks of homogeneous velocities. The parameterization in spherical coordinates accounted for the curvature in block surfaces. Following the work of *Aki and Lee* [1976], the relation between data and model parameters was linearized,

$$\Delta d = G\Delta m, \tag{1}$$

where Δm is the adjustment of model parameters, G is the matrix of partial derivatives calculated in reference to the last updated model, and Δd is the variation in arrival times. The analytical values for the derivatives are described by *Thurber* [1983].

The damped least squares method [*Maquardt*, 1963] was used to produce the system of normal equations,

$$(G^t G + \theta)\Delta m = G^t \Delta d, \tag{2}$$

were θ is the diagonal matrix of damping factors.

Equation (2) is solved by triangularization to obtain the model variations. The model is updated by

$$m_1 = m_0 + a\Delta m, \tag{3}$$

where the scalar a is a step-size damping factor. Whereas the damping factors θ are constant values throughout the inversion, the step-size damping factor a is selected at each inversion step by trial and error, between bound values from zero to one, to minimize the misfit between calculated and observed data. The step-size damping factor adapts the size of the model adjustment Δm resulting from the linear regression to the nonlinear effects, preventing underdamping. This is not important in the 3-D inversion and resulted in values of 0.98 and 0.89 for the two iteration steps used but is very important in the 1-D inversion where nonlinear effects are stronger, producing smoother and faster progress in misfit reduction.

The travel times were calculated by ray tracing, following a method similar to the one by *Horie* [1980] and *Thurber and Ellsworth* [1980], extended to spherical coordinates by *Ishida and Hasemi* [1988]. The method provides fast and sufficiently accurate arrival time calculation and has been widely used in local earthquake tomography for these reasons. It consists basically of (1) calculating the ray path by iterative shooting in the 1-D background velocity model, (2) calculating travel time for the 3-D velocity model following the 1-D path, and (3) making this calculation for the direct arrival and all refracted arrivals and selecting the smallest one. As lateral velocity variations are smaller than vertical variations, the 1-D ray path is a good approximation of the exact 3-D ray path, and according to Fermat's principle the calculated arrival time should be a good approximation of the exact arrival time as well. *Hasemi and Ishida* [1987] provide detailed tests and descriptions of the technique with synthetic data and real data from the Japan area.

The inversion of arrival times was performed in two stages: (1) estimation of a vertical 1-D velocity model and (2) estimation of lateral heterogeneities. Many researchers [see *Kissling et al.*, 1994] have shown that the selection of an appropriate 1-D velocity model is critical for the estimation of the 3-D heterogeneities. The distinction between the two stages results from the velocity structure of the crust and mantle. With the exception of the first few kilometers the vertical velocity variations are much larger than the lateral velocity variations. As a consequence a smaller number of velocity parameters with strong nonlinear behavior are estimated in the 1-D inversion. In this case the inversion is often long and complex, whereas in the 3-D stage the velocity parameters behave close to linearity, and convergence can often be achieved with a few iterations.

Original work by *Aki and Lee* [1976] considered the simple case of homogeneous media and fixed earthquake source parameters. Early, it was generalized to spherically layered media and simultaneous inversion of earthquake sources and velocity variations [*Hirahara*, 1977]. Here the model parameters adjusted by the inversion Δm include source locations (hypocentral coordinates and origin time), block velocity variations relative to the 1-D velocity model ($\Delta V/V$), and time corrections for the stations. Time corrections for stations were not applied for the 1-D inversion to avoid the

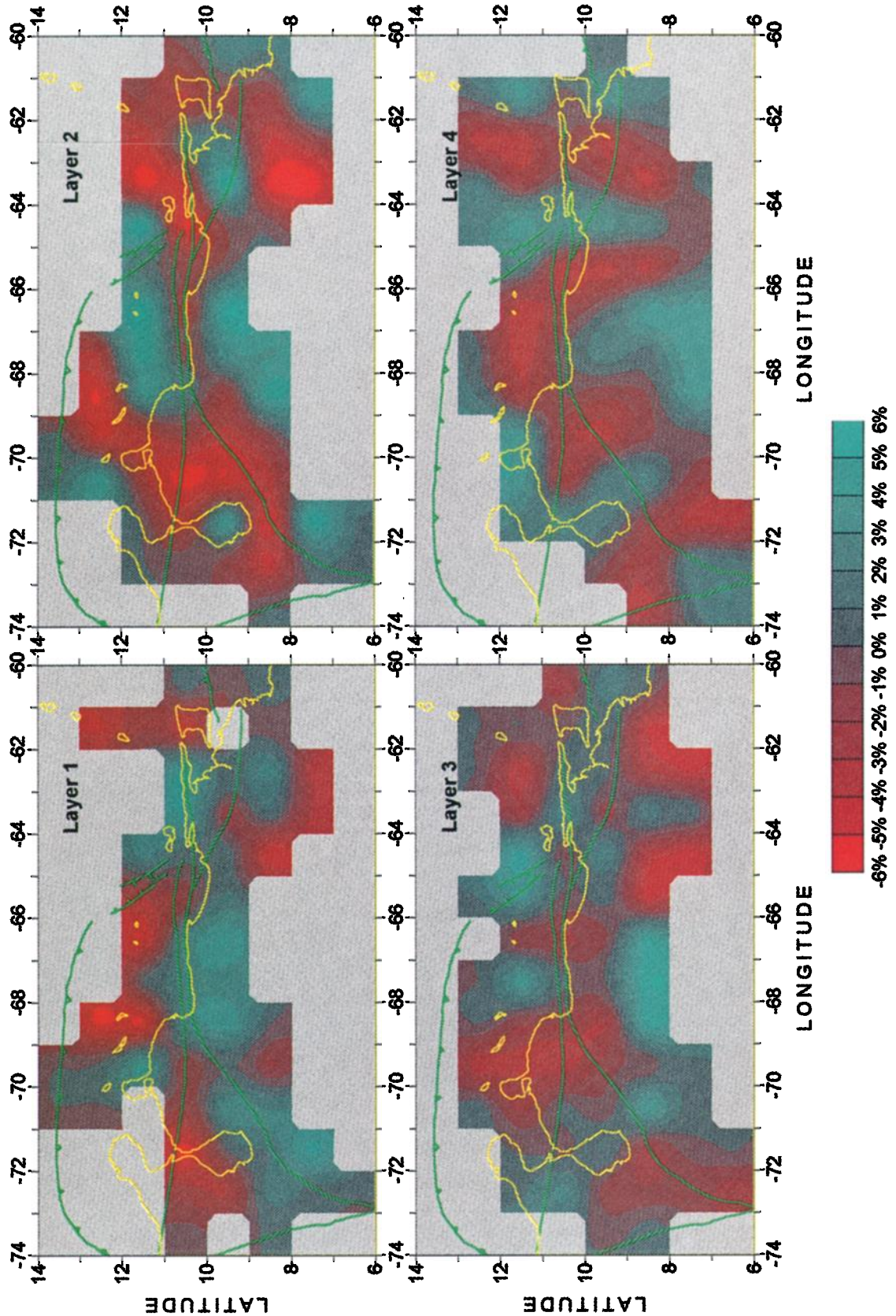

Plate 1. Contour maps obtained from the block velocity result for each of the four layers. Percent velocity variations are relative to the 1-D velocity background model (Figure 3g). The coastline is in yellow, and the relevant fault systems are in green. Clear gray areas represent unsampled blocks.

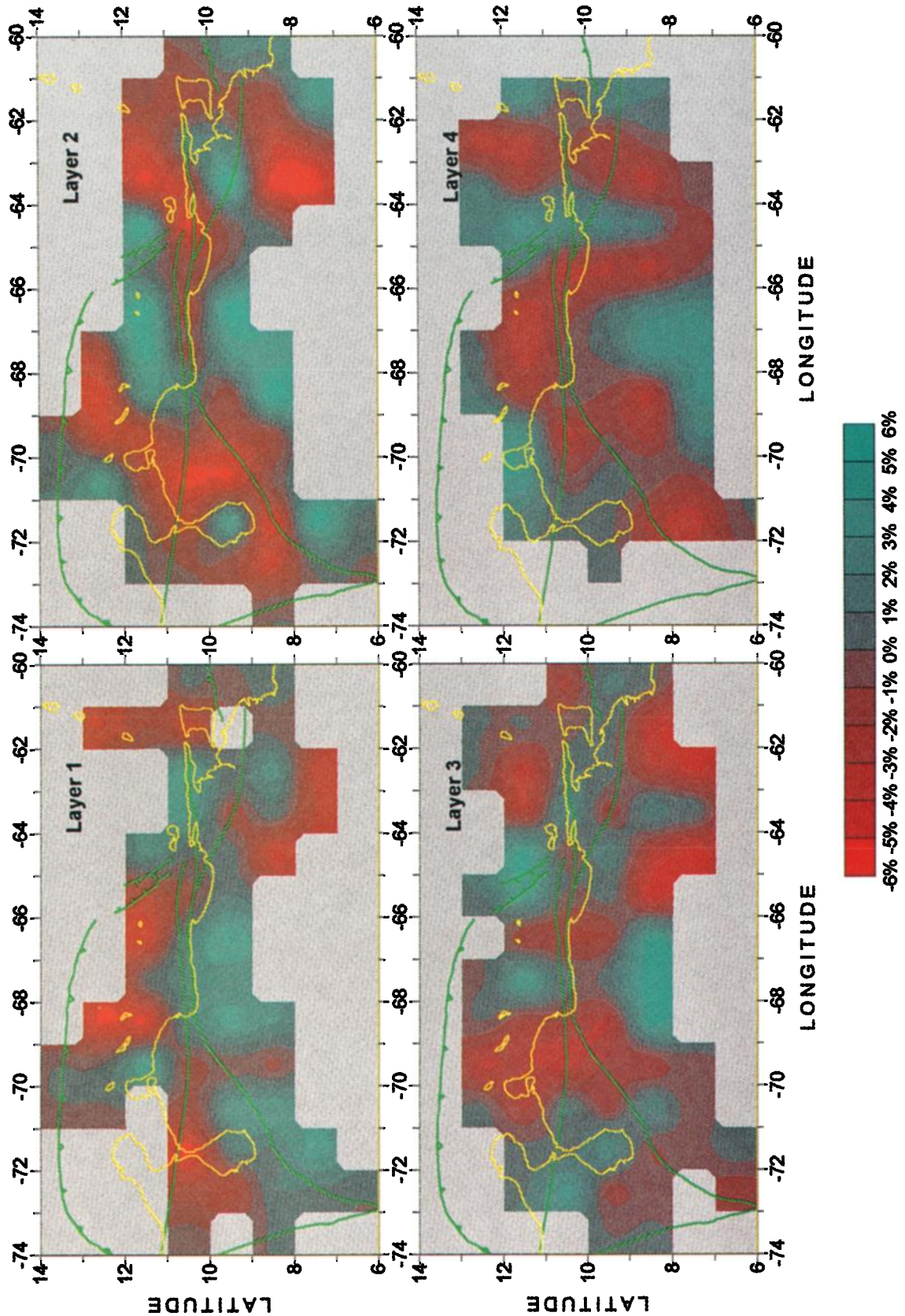

Plate 2. Results from the inversion without Bucaramanga events. A reduced data set was created removing all events from the Bucaramanga and adjacent areas (grey zone of Figure 2). The reduced data set was inverted following the same procedure (same damping parameters and two iterations) as for the normal inversion of Plate 1.

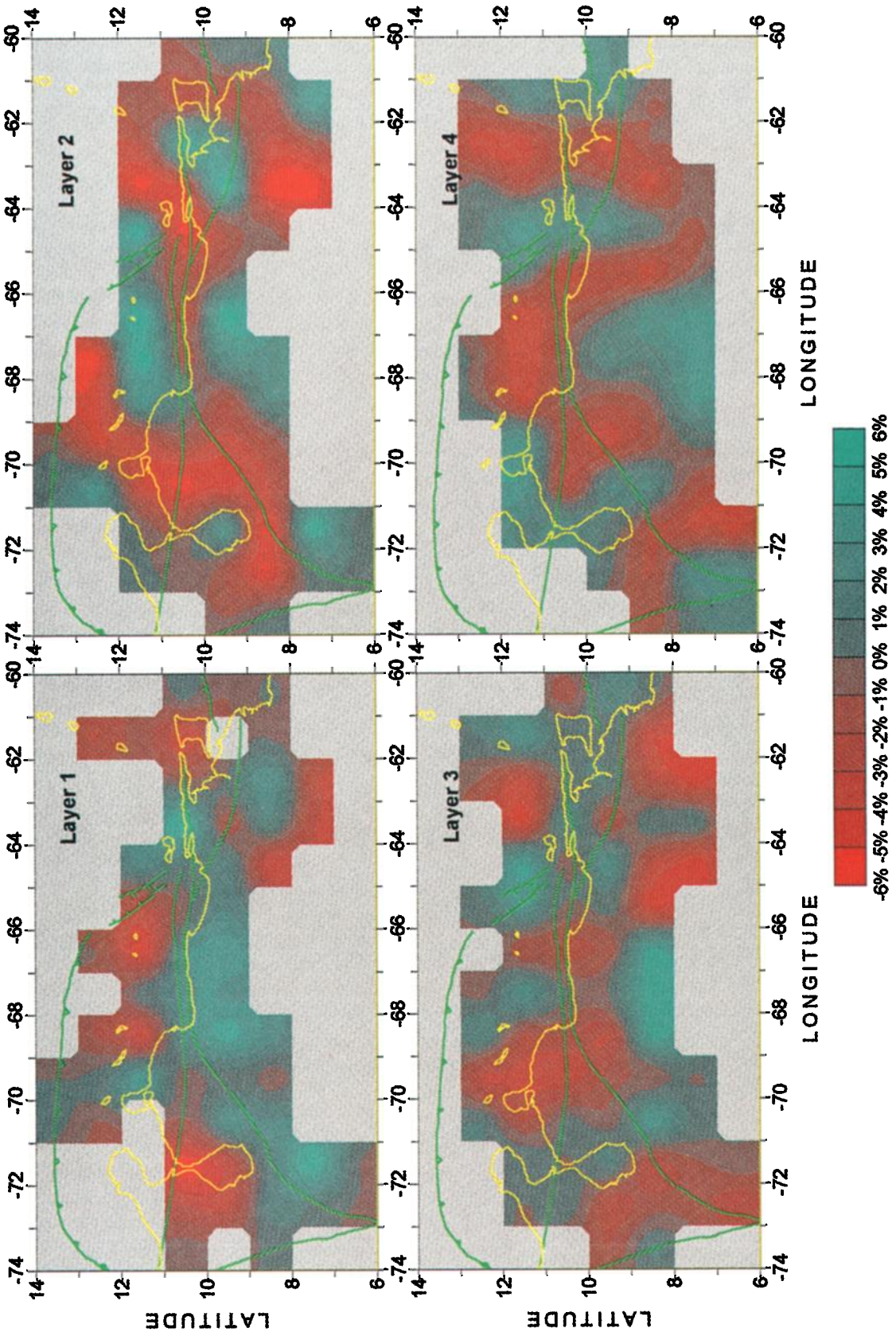

Plate 3. Results from the inversion of the complete data set providing incorrect initial source locations to the inversion algorithm. The initial source locations, as obtained at the 1-D inversion, were modified by large Gaussian-distributed displacements with standard deviations of 5 km for coordinates and 0.5 s for origin time. The inversion proceeded with the same damping parameters and two iterations as for the normal inversion.

assimilation of time delays associated with the 3-D velocity structure. In the 3-D inversion, station corrections were properly damped in order to maintain small values in accord with the size of expected local delay effects in the area. After the 3-D inversion, station corrections resulted in values below 0.2 s with average absolute value of 0.08 s.

Damping factors in (2) were selected by

$$\theta_m = \sigma_d^2/\sigma_m^2, \quad (4)$$

where σ_d and σ_m are prior selections for the standard deviation of the data and the standard deviation of the model parameter m, respectively. The damping factors used in the 3-D inversion corresponded to standard deviation values of 0.2 s for arrival times, 0.05° for latitude and longitude hypocentral coordinates, 5 km for hypocentral depth, 0.025 for the relative velocity variation ($\Delta V/V$), and 0.07 s for time station corrections. Different variations around those values were tried and the misfit reduction examined. Described values correspond to the combination producing better results in residual reduction. In the 3-D inversion all parameters (sources, velocity variations, and station corrections) were jointly inverted, and convergence was obtained for the second iteration. In the 1-D inversion several consecutive steps of source relocations (until source relocation converged) were combined with steps of joint velocity and source inversion, using stronger damping factors for the source parameters (4 times larger) than the ones used in the 3-D inversion.

Simple representation of the media by regular blocks has been commonly used in local seismic tomography to determine the velocity structure at lithospheric ranges. An important comment is whether the Moho depth variations can be included in the model or whether they can be also inverted from data. Inclusion of three fixed discontinuities into the model (Conrad, Moho, and a suducting slab) was carefully done by *Zhao and Hasegawa* [1993] in a *P* wave tomographic imaging of the crust and upper mantle beneath the Japanese Islands. The authors considered the geometry of these discontinuities, given by previous geophysical studies in the area, adapting block boundaries to follow them. They inverted block velocity variations from data, with no modification of block geometry throughout the inversion. Following the same method, the authors inverted the data considering the Moho and Conrad discontinuities as spherical surfaces, concluding that the general pattern of the inverted velocities in the two results was almost the same. On the other hand, they found that the inclusion of the slab discontinuity was significant for the inversion of the velocities in the Pacific area below the slab. It is important to mention that Moho variations in the Japan area, considered in Zhao and Hasegawa's work, are stronger than the ones in the Venezuelan area.

The inclusion of Moho depth geometry in the model according to the *Zhao and Hasegawa* [1993] method has the additional complication that the geometry of discontinuities should be very well known in the area. On the other hand, the alternative of including Moho depth as new parameters in the inversion has additional problems, because Moho depth and block velocity below Moho have very similar effects in data prediction. An increase of Moho depth will produce a delay in arrival times for rays crossing it, both for direct and refracted phases. The same effect in arrival times would be produced by a decrease in the velocity below Moho, and hence the phenomena are indistinguishable by means of first arrival times. The introduction of additional parameters into a model, incrementing the number of variables to estimate with the same amount of data, is only justifiable if they provide independent predictive abilities to the model.

The 1-D Velocity Model

The current velocity model used by the network for foci determination was first proposed by *Perez and Aggarwal* for a local area of eastern Venezuela. Some other models have been proposed by *Castejón et al.* [1986] and *Mendoza* [1989] for local areas inside the Venezuelan region. Here the reduction of the misfit between calculated and observed data and the simplicity of the model were used as criteria in order to select an appropriate 1-D background velocity model.

Arrival times were inverted using several different initial velocity models (see Figures 3a-3c). Velocities for 11 homogeneous layers, bounded at fixed depth, were estimated from the data, following a combination of iterative steps of source location (hypocentral location and origin time) inversion, simultaneous source location and velocity inversion, and model regularization. A detailed description of the procedure is found elsewhere [*Bosch*, 1994].

The most important features present in the solutions (Figures 3d-3f) were identified and used to construct a representative model of the velocities (Figure 3g) that will be called the proposed model. It produces a very good reduction of the residuals, when compared to any of the initial models. On the other hand, the misfit reduction produced by the different inverted models (Figures 3d-3f) and the proposed model are all similar, showing that lateral homogeneous models were unable to significantly improve the residuals.

The proposed model shows deeper discontinuities than the Perez and Aggarwal's [1981] model (Figure 3a); typical mantle velocities of 8.2 km/s are present below the depth of 50 km. A layer with velocity of 7.5 km/s is present between 30 and 50 km depth. This intermediate velocity layer may be explained as a pondered average due to lateral variations of Moho at this depth. The Moho variations throughout the study area have been estimated to be significant, ranging between 20 km and 40 km depth [*Case et al.*, 1990; *Bosch and Rodríguez*, 1992].

The velocity of 6.0 km/s at 30 km depth is an average crustal velocity. No internal discontinuity in the velocity of the crust to 30 km was found to be important enough to explain the arrival times over the area of study. Most of the area is of accretional origin and therefore a continuous intracrustal discontinuity along the study area (like the Conrad discontinuity) is not expected.

The 3-D Velocity Inversion

On the basis of the four-layer model selected in the first stage of inversion, the joint inversion of the *P* wave veloc-

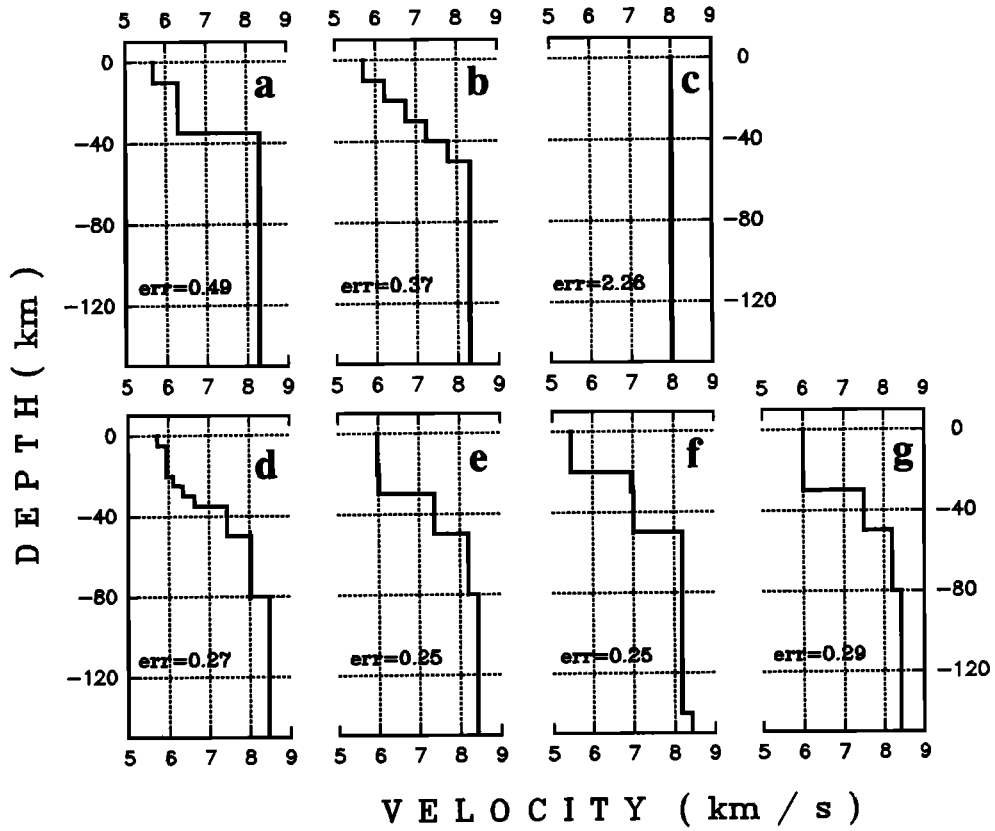

Figure 3. Initial velocity models before the one-dimensional (1-D) inversion are shown (top) in figure 3. (a) The model used by *Perez and Aggarwal* [1981] for the northeastern region of Venezuela, (b) a regular stair model, and (c) a constant velocity model were used. (d-f) The inverted 1-D velocity models are shown (bottom) in figure 3, below each corresponding initial model. (g) The representative model was constructed from the common features observed in the different inversion solutions. The source locations (hypocentral locations and origin times) were relocated according to each velocity model under consideration. The error indication corresponds to the average quadratic misfit after the relocation.

ity variations, source locations, and time corrections for the stations was performed. Special attention in this work was directed to the study of the power resolution of the data set and the method on the velocity structure to assure that an appropriate estimation of the block velocities was attained. The framework considered in this work to assess the confidence in velocity estimates consisted of a complete series of tests including the following: (1) statistical significance of the misfit reduction via the F test, (2) calculation of the resolution matrix and the variance-covariance matrix, (3) checkerboard synthetic inversions with and without noise in data and perturbation of source locations, and (4) several modifications to the data set to study the robustness of the solution under the elimination of quakes coming from particular areas, perturbation of the initial source locations, elimination of largest residuals, and other cases.

From the work of *Aki and Lee* [1976] the calculation of the resolution matrix [*Wiggins*, 1972] and the variance-covariance matrix were introduced as a means to analyze the resolution and uncertainties in the inversion results according to the geometry of the problem and the spatial model resolution selected. Analysis based on such matrices has the advantage of taking into account, in a quantitative way, the complex relation between all parameters involved in the linear regression but the disadvantage of neglecting the nonlinear aspects of the inversion. Because of the impossibility of performing these calculations in large tomographic problems, treated by iterative matrix solvers, synthetic resolution tests were developed, the best known of these is the checkerboard test [*Humphreys and Clayton*, 1988]. These tests had the advantage of including nonlinear effects of the modeled wave propagation but the disadvantage of evaluating particular synthetic situations. All these tests allow the analysis of different aspects of the confidence on inverted estimates and should, in fact, be used together as in this work.

The reduction in the sum of squared residuals achieved in the 3-D inversion stage was 49%, which is highly significant following an overall F test. The F test is a statistical tool that measures the significance of new parameters added into a linear regression problem, according to the amount of data, the total amount of parameters, the amount of new parameters introduced and the residual reduction achieved. The F ratio [see *Myers*, 1986] is known to be

$$F = \frac{(SSR_1 - SSR_2)/(DF_1 - DF_2)}{SSR_2/DF_2},$$

where SSR is the sum of squared residuals and DF is the number of degrees of freedom (number of data minus number of unknown parameters). Subscript 1 refers to the reduced model (without additional unknown parameters), and subscript 2 refers to the complete model (with the additional unknown parameters). The F test comparing the 3-D inversion result (complete model) with the source inversion result using the background 1-D model (reduced model) provided a probability below $p = 10^{-5}$ for the so-called null hypothesis, which is the hypothesis that new estimated parameters (block velocities and station corrections) are not significant to explain the data.

The F test is a tool for linear regression, and it can lead to erroneous interpretations in the nonlinear case, but it can be used with approximation at the 3-D inversion stage since it behaves close to linearity. The F test was also used as a guide for tuning the spatial model resolution: the significance of residual reduction decreased when more unknown parameters were added to the model by reducing the size of the blocks or by introducing additional layers.

The checkerboard test without addition of noise was performed generating synthetic arrival times for an alternate pattern of $\pm 3\%$ of relative velocity variation. Arrival times were calculated for the same pairs source station present in the inversion data set, using same source locations provided by the 1-D inversion. These synthetic data were inverted following identical procedures (same damping parameters, starting source locations, and two iteration steps) as the ones used in the inversion of observational data. If a block is sampled by rays in many different directions, the inversion algorithm will be able to estimate its velocity independently from neighboring blocks. On the contrary, if a block is sampled by few rays or by many nearly parallel rays, the block could not be well differentiated from neighbors, and the velocity pattern would be smoothed between neighboring blocks. This test essentially shows if the path geometry produces independent information allowing adequate solution for block velocities.

Figure 4 shows the result obtained by the checkerboard test without the addition of noise. Good recognition of the alternating pattern is shown for the different layers, with the exception of poorly sampled blocks in the borders of the resolved volume. Also, the raypath coverage (sampled and nonsampled blocks) is illustrated in Figure 4. The horizontal distribution of the resolution and coverage follows the irregular distribution of sources and stations in the area. With depth the resolution and coverage show adequate sampling penetration up to the deepest layer, with the best pattern recovery for layer 3.

Figure 5 shows the result of a similar checkerboard test which includes noise in arrival times and perturbation of the initial source locations. Comparison with the checkerboard test without noise allows the evaluation of the sensibility of block velocities estimated by the algorithm to data errors and to wrong 1-D location of sources. For this test, synthetic arrival times were calculated in the same way as before and for the same locations as provided by the 1-D inversion. Then, Gaussian noise with 0.1 s standard deviation was added to the data. The inversion procedure was the same as the test without noise (same damping parameters and two iterations) but providing the inversion algorithm with very erroneous starting source locations. Starting source locations were perturbed following a Gaussian distribution with standard deviation of 5 km for coordinates and 0.5 s for origin time. The results are very similar to the test without noise, showing some amplitude changes and degradation of pattern recognition only in poorly sampled blocks.

The 3-D velocity model obtained from the inversion of the observed data, the results of the calculation of the diagonal element of the resolution matrix, and the standard deviation obtained from the variance-covariance matrix are described in Figure 6. Blocks with the diagonal element of the resolution matrix lower than 0.1 are mostly coincident with the blocks showing inadequate pattern recovery in the checkerboard tests. They are located at the borders of the covered area. In order to facilitate the interpretation of the results obtained from the inversion, contour maps are shown in Plate 1 for the velocity lateral variations.

To examine the possibility that systematic errors in source locations could be influencing the velocity estimations, a group of earthquakes located at the southwestern corner of the studied volume were removed from the inversion data set. All data from earthquakes originated in the Bucaramanga nest area (grey area in Figure 2) were excluded from the inversion. Earthquakes from the Bucaramanga zone are a significant 20% of the events considered in the inversion, providing direct arrivals to stations at western, central, and eastern Venezuelan area. They are located in the periphery of the array and may be suspected of being less accurately located than other events in the area. In fact, the largest source standard deviations calculated from the variance-covariance matrix belong to events within this area. Nevertheless, with all these considerations the inversion results without Bucaramanga data (Plate 2) showed no significant changes in velocity structure from the inversion using the full data set, with the natural exception of the reduced coverage in the southwest area of layer 4. This is an indication of significant robustness of the solution and, in particular, shows that possible errors in source locations of Bucaramanga's quakes are not introducing bias into the velocity estimation. Also, this shows that information on the velocity provided by direct paths of Bucaramanga's earthquakes is very consistent with the information from refracted path of shallower quakes.

Similar tests removing earthquakes from different peripheral locations at the northeastern and western areas were performed with similar results, demonstrating that posible errors in locations were not significantly affecting the estimation of velocity structure in the area. To further examine this consideration, a different test was performed regarding the consequences on the velocity inversion of having significant random errors in the original locations provided by the 1-D velocity inversion. The inversion was performed using the full data set and the same procedure (same damping parameters and two iterations), but erroneous initial source locations were provided by adding Gaussian-distributed perturbations with standard deviations of 5 km for hypocentral coordinates and 0.5 s for origin times to the source locations provided by

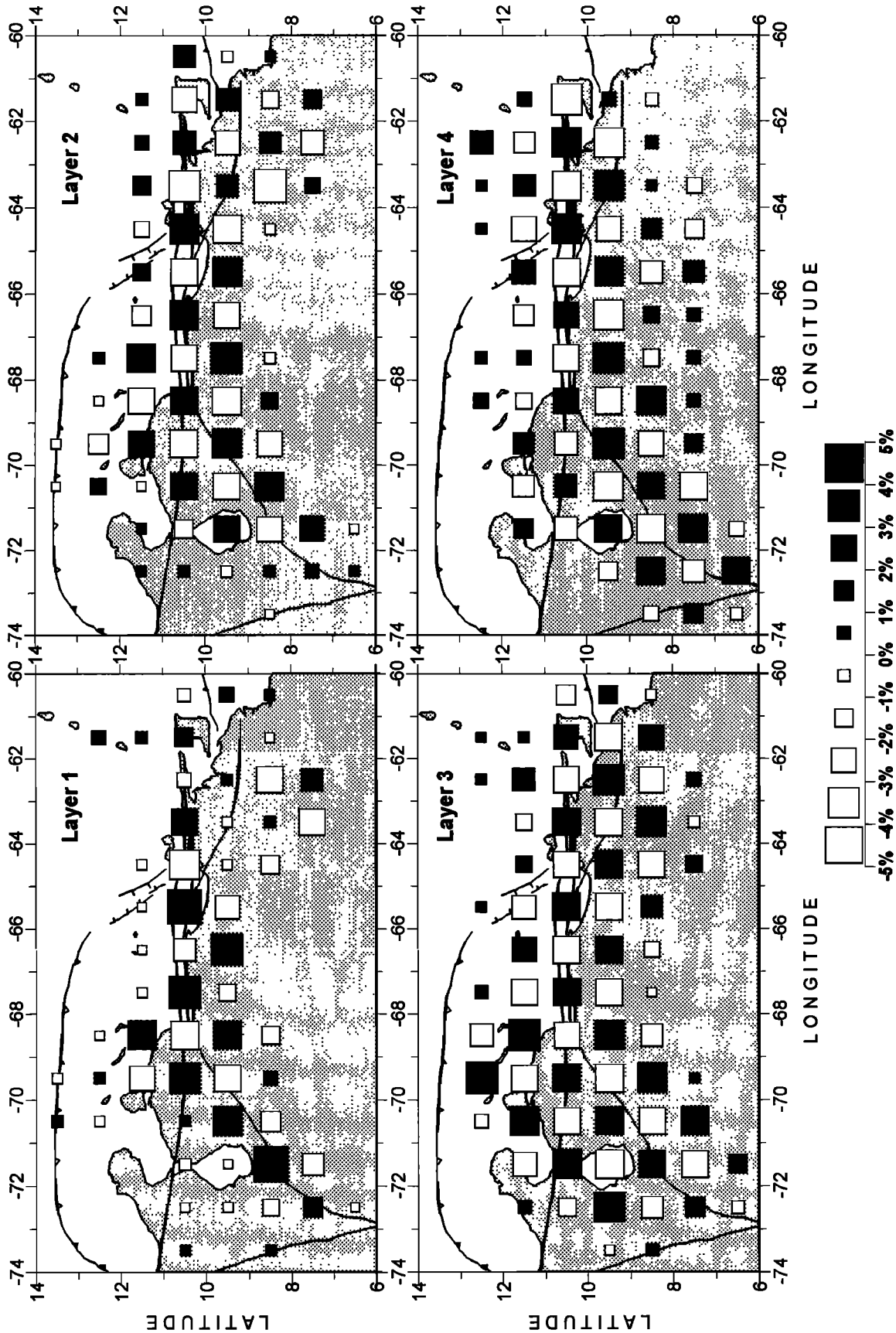

Figure 4. Checkerboard velocity resolution test. Synthetic arrival times were generated at the same ray geometry defined by the data for a ±3% alternating velocity variation model. Percent velocity variations are relative to the 1-D background velocity model (Figure 3g). The synthetic arrival times were inverted in two iterations, and the results were presented for each of the four layers. White and black squares denote high and low velocities, respectively. Areas without squares indicate nonsampled blocks. The alternating pattern is recovered, except for poorly sampled border blocks, showing that the geometry of the tomographic problem is able to resolve the block velocities. The coverage is also shown reaching a maximum for layer 3.

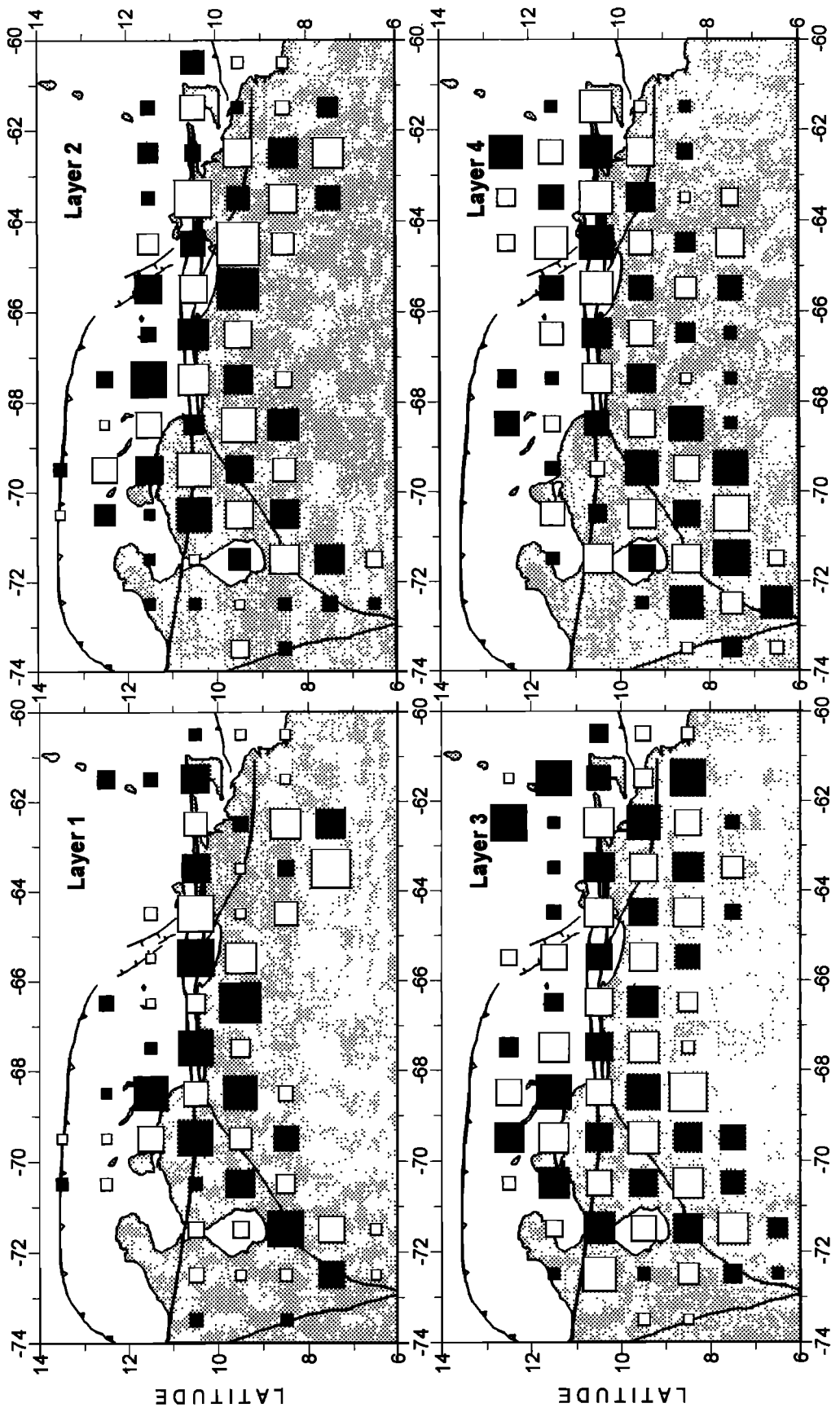

Figure 5. Results for a checkerboard velocity resolution test with added Gaussian-distributed noise with standard deviation of 0.1 s in arrival times and Gaussian-distributed displacement of standard deviations of 5 km for coordinates and 0.5 s for origin time in initial source locations. The inversion followed the same procedure (same damping factors and two iterations) as for the test without noise. The alternating pattern is recovered, except for poorly sampled blocks located at borders of the sampled volume.

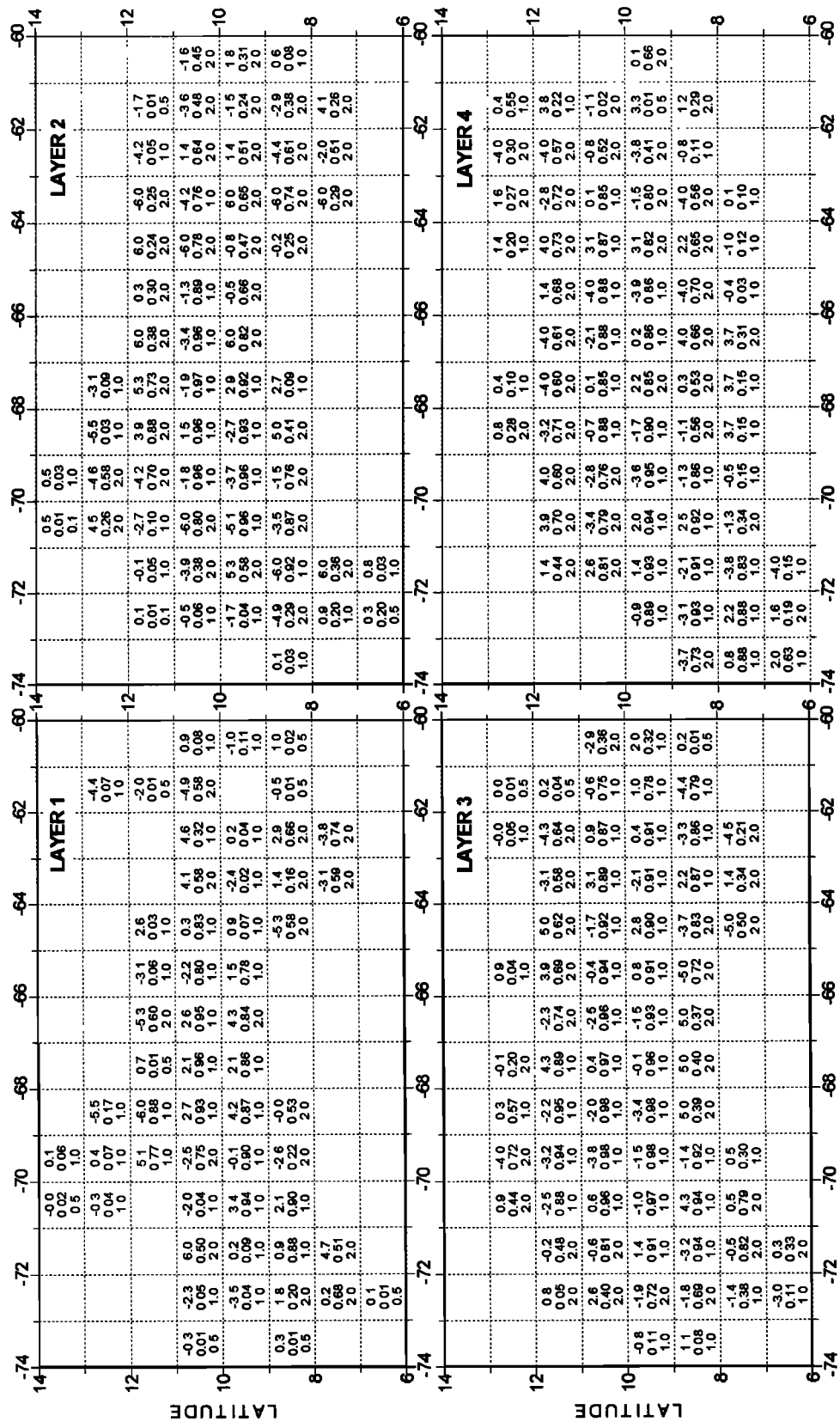

Figure 6. Results of the inversion. The model blocks are separated by dotted lines. The upper number at each block corresponds to the estimated percent velocity variation relative to the background 1-D velocity model. The lower number is the standard deviation of the later from the variance-covariance matrix. The middle number is the diagonal element of the resolution matrix. Unsampled blocks are not filled. The depth of the layers are as follows: layer 1, 0-30 km depth; layer 2, 30-50 km depth; layer 3, 50-80 km depth; and layer 4, more than 80 km depth.

the 1-D inversion. It is important to note that these perturbations are larger than the uncertainties predicted by the variance covariance matrix of the 1-D inversion. The result of this test (Plate 3) produced a very similar velocity image to that of the normal inversion thus confirming the robustness of the inversion to changes in initial location of sources.

Another problem present in least squares inversion is the robustness to large residuals. As the L_2 norm is used, possible outliers can drastically influence the solution. To test the robustness of the results, a trimmed inversion was performed (up to 4% of the paths with larger residuals were removed from the inversion), producing similar results in velocity images. In this way it was shown that the solution was not significantly affected by possible errors in data or by other kind of outliers.

Discussion

The velocity images resulting from the inversion were compared to the geology of the area and to other geophysical information. As the block velocity represents an average velocity in ray paths within the block, heterogeneous structure inside the block is averaged. For the spatial resolution used in this work, stratigraphic features should be reflected in the lateral variations of the block velocities at the crustal layer. A deep sedimentary basin will contribute to lowering the average velocity in the corresponding crustal block, and a mountain chain will contribute to increasing it, as the sedimentary cover is absent. Likewise, at Moho depths the Moho variations should influence the lateral variation of block velocities; low velocities are associated with a deeper Moho, and high velocities correspond to a shallower Moho depth. At crustal depths (layer 1, Plate 1) the major mountains of Venezuela (the Venezuelan Andes, the Coastal Chain, and the Eastern Chain) are associated with high-velocity zones. On the other hand, the deepest basins (Maracaibo, Cariaco, Bonaire, and Eastern Venezuela Basins) are associated with low-velocity zones. However, a part of the Eastern Venezuela Basin exhibits moderately high velocities, which will be discussed later.

Velocities of the layer bounded between 30 and 50 km depth (layer 2, Plate 1) were compared to the Bouguer Anomaly Map of the region (Plate 4). The correlation, at long wavelengths, can be explained because both maps are strongly influenced by Moho depths, characterized by discontinuities in density and seismic velocity. The Bouguer anomaly is also influenced by the sedimentary cover and other heterogeneities above 30 km depth, which is not the case for the velocity of the layer 2, which is located between 30 km and 50 km depth. A moderate low-velocity zone is shown along the Coastal Chain connecting to a larger one along the Venezuelan Andes; the minimum is located to the west of the Venezuelan Andes. These features can be found on the Bouguer Anomaly Map and are well explained [*Bosch and Rodríguez*, 1992; *Kellog and Bonini*, 1982; *Case et al.*, 1990] by the variation in Moho depth. The correlation between the gravity and the velocity is inverted in the Eastern Venezuelan Basin. A high-velocity zone is superimposed over the largest negative continental gravity anomaly. The gravity minimum is too large to be explained by crustal flexure alone. The model of an oceanic subducted slab, overridden by continental South America, has been proposed to solve this problem [see *Russo and Speed*, 1992, 1994]. The high-velocity zone shown below the Eastern Venezuelan Basin could be explained by this kind of model. The Atlantic lithosphere originally attached to the South American continent along the coastline has been subducted below the Caribbean plate at the Lesser Antilles island arc. Russo and Speed's model considers that this oceanic subducted lithosphere has been detached from the adjacent continental lithosphere and has been overridden by the South American continent in its movement to the northeast with respect to the mantle. As a result the oceanic lithosphere originally at the northern margin of the South American continent would be now below it, with the top of the slab projecting along a line directed to the southwest.

The anomalous correlation of gravity and the velocity in the area below the Eastern Venezuelan Basin can be explained by this model. The subducted lithosphere introduces changes in the isotherm to colder temperatures below the area and hence higher velocities. However, density decreases (the opposite behavior) because the low density of subducted oceanic crust introduces a deficit of mass in the area. To make a more precise comparison between the seismic velocity results and the gravity in the area, block densities were estimated from block velocities, and the Bouguer anomaly was calculated. For the calculation of densities from P wave velocities the formula

$$\rho = a + b/V_p \tag{5}$$

was used, where the coefficients a and b were estimated for different depths [*Christensen and Mooney*, 1995]. It is important to notice that coefficients for each depth were obtained for fixed average conditions of temperature and presure, not including effects of temperature or lithological lateral variations. The results, shown in Plate 4 correlate with the observed Bouguer Anomaly Map (same Plate 4, top), maintaining the anticorrelation at the northeastern area, which is the expected result for a slab subduction phenomena.

Velocities corresponding to the lithosphere below the Moho show an interesting relation with the tectonics. The most significant feature in the layer bounded between 50 and 80 km depth (layer 3, Plate 1) is a wide low-velocity zone below the triple junction of the fault systems of Boconó, Oca, and Morón, in northwestern Venezuela. The area over the low-velocity zone was subjected to significant crustal extension during Oligocene and Miocene times [*Muessig*, 1984]. The low-velocity zone may be associated with higher temperatures in the lithosphere. Higher temperatures could be caused by extensional deformation due to the complex interaction between the Maracaibo Block, the Bonaire Block, and the South American plate (for results on Global Positioning System measurements and a recent review on kinematics see *Freymueller et al.* [1993]). Also, underlying mantle convection phenomena could explain higher temperatures in the lithosphere.

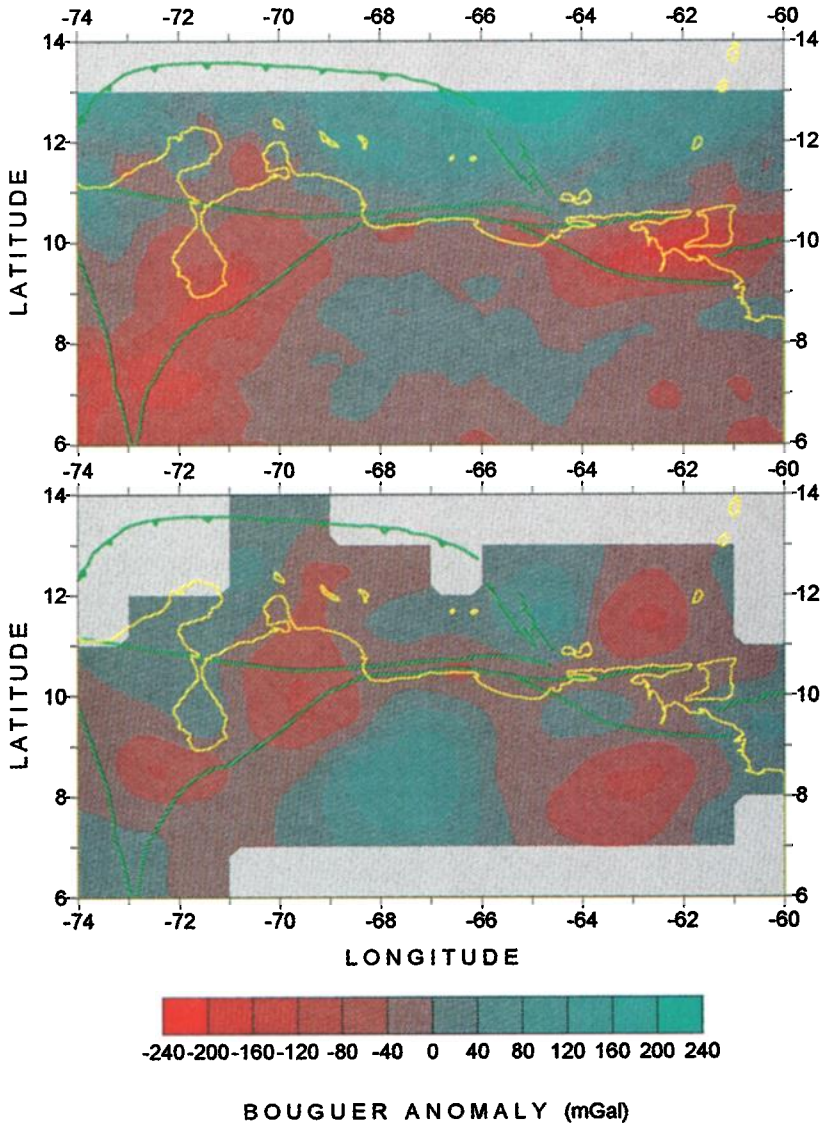

Plate 4. (top) The Bouguer Anomaly Map for the study region ($p = 2.67$ Mg/m^3) based on the map compiled by *Graterol* [1988] is shown. (bottom) The Bouguer Anomaly calculated from the P wave block velocity results obtained by the inversion after conventional conversion to block densities is shown. The gravity effect of the four layers is included. The calculated anomaly is only shown over blocks with estimated velocity variations.

The velocities for the deepest layer in the model (layer 4, Plate 1) show a connection of the low-velocity zones along the trend of the Boconó-Morón fault system. The southern corner of the Maracaibo Block is also near a low-velocity zone at the confluence of two low-velocity trends extending beside the Santa Marta fault system and the Boconó fault system. A low-velocity zone also is present at the eastern limit of the Bonaire Block besides the La Orchila fault zone. The normal faults enclose a rectangular basin, La Orchila Basin, joining the South Caribbean Marginal Fault to the north and the Morón-El Pilar fault system to the south. The rifted basin resulted from E-W extensional stress and deformation during Oligocene and Miocene [*Muessig*, 1984].

The relative motion between the Caribbean and the South American plates is accommodated by several blocks occupying a wide area of interaction. Most of the motion and deformation takes place at block boundaries, generating the Venezuelan Andes and the Coastal Chain at the continental borders. It has been well established that active mountain belts are weak zones of the lithosphere [*McNutt et al.*, 1988]. The stress produced by the load of the belt and the flexure of the lithosphere [*Burov and Diament*, 1995] and the radiogenic heat in the belt [*Huerta et al.*, 1996] are able to radically reduce the strength of the lithosphere. Hence it seems clear that the lithosphere in block centers should be more competent and stable than in block boundaries. Tomographic images of the region show that compressional velocity variations below the Moho are associated with the geodynamic setting of the plates. A decrease of the order of 4% of the velocity is identified at the zones below or near multiple junc-

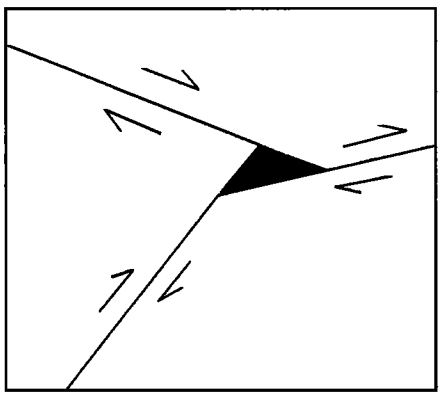

Figure 7. Relative movement between microplates is able to create local extension (see black area) at the junctions. The movement represented would be the response to compression in the horizontal axis direction of the figure 7 with no thrusting between microplates.

tions of the fault systems bounding the blocks. Also, a smaller velocity reduction seems to follow the strike-slip block borders below 80 km depth.

Low-velocity zones at block corners may result from local lithospheric extension. Even though the regional setting of the area is compressive, local extension can be produced by the displacement of blocks. In particular, if thrusting is limited by friction or buoyancy, the compressional forces may produce divergence of blocks in block corners (triple junctions) as shown schematically in Figure 7. Local lithospheric extension, or buildup, taking place at block corners would be able to explain higher thermal flux, higher temperatures, and the lower compressional velocities at the subcrustal lithosphere.

A latitudinal depth section of the area is shown in Plate 5. It is possible to see that all structures show vertical continuity below 30 km depth. Above this depth, crustal heterogeneities dominate the velocity variations. Previously, the relation of low-velocity zone (LVZ)1 and LVZ2 (see Plate 1) in the subcrustal lithosphere with the crustal fault systems of Santa Marta and Boconó has been discussed. These two hot zones enclose a colder stable lithosphere high-velocity zone (HVZ)1 at the base of the Maracaibo Block. The HVZ2 represents colder lithosphere below the shallow basin of Los Llanos, a stable zone. HVZ3 was mentioned previously as an indication of an overridden slab interpreted from gravimetric and geologic information. HVZ4 can be interpreted as a progression to thinner oceanic lithosphere.

Other tomographic studies overlapping the volume considered in this work are of a different scale. *Franke* [1994] used arrival times from a microseismic campaign along the El Pilar fault, estimating seismic velocities to a maximum depth of 20 km. The studied volume is enclosed in two blocks of the first layer of the present inversion, not allowing for a useful comparison. A study by *Van der Hilst* [1990] used teleseismic trajectories of Caribbean earthquakes to the world-wide seismological network to estimate compressional velocities in the Caribbean region to a depth of 1325 km, separated in 15 layers; the studied volume was 2 orders of magnitude larger than the one considered here. Although there was a difference in spatial resolution and sensitivity, images

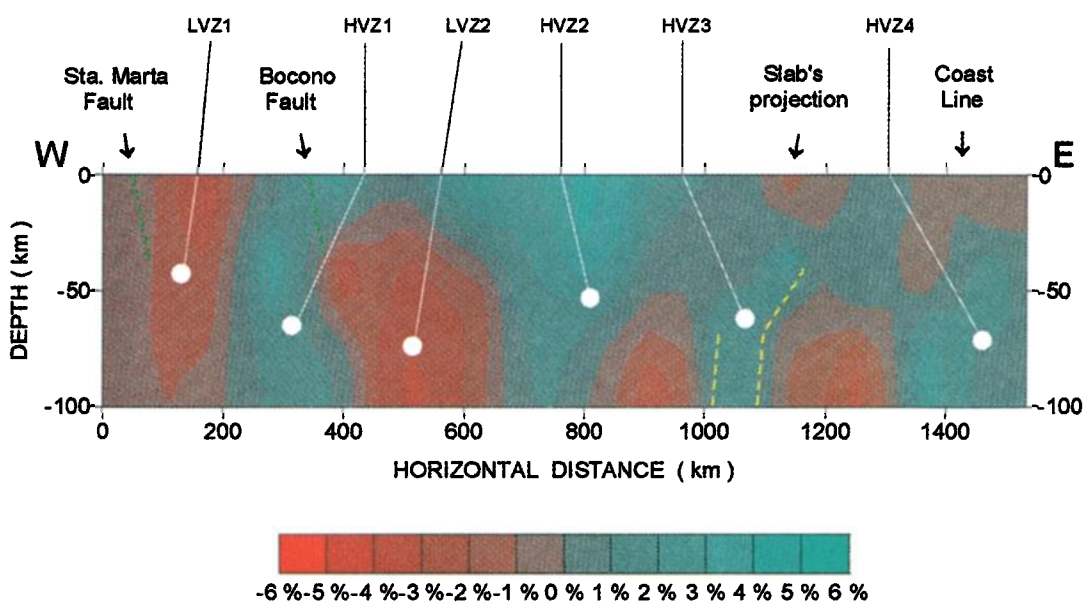

Plate 5. Vertical depth section of the percent velocity variation along the parallel 9.5°. Continuity in depth of the structures below 30 km (subcrustal lithosphere) is shown by the cross section. LVL means low-velocity zone, and HVZ means high-velocity zone. Arrows indicate the intersection with fault traces, the coast line, and the trace projected to the surface of the proposed oceanic slab according to *Russo and Speed* [1992]. Vertical exaggeration is of the order of 4 times.

can be compared showing similarities. In particular, below 80 km depth (Van der Hilst's layer 3), the low-velocity zone along the Boconó-Morón fault system was resolved, and the two minima associated with the corners of the Maracaibo Block can be identified. Comparison to Van der Hilst's layer 2 is difficult because it intersects layers 2 and 3 of the present work, but the high-velocity zone below the Eastern Venezuelan Basin is not observed. Van der Hilst's crustal layer (layer 1) shows a pattern correlated to the main stratigrafic features, approximately similar to those presented here.

Conclusions

Arrival times from the local seismological network of Venezuela were inverted to produce velocity images of the lithosphere in the region along the boundary between the Caribbean and the South American plates. Although the spatial distribution of quakes and stations is irregular, a significant area was covered to more than 80 km depth.

A 1-D background velocity model was first optimized in order to adequately represent the main vertical variations in the area. This model showed a deeper crustal structure and a much better error reduction than the previous crustal models for the area.

The lateral velocity variations estimated by the 3-D inversion were very significant to explain the observed arrival times in the area, as was demonstrated by the overall F test. The resolution for each block velocity estimation was tested by the checkerboard synthetic tests and by the calculation of the resolution matrix. With the exception of border blocks, block velocities were well determined by the ray geometry and the amount of data collected. Finally, the solution proved to be considerably robust to the influence of the hypocentral locations errors for the events considered in the inversion.

Results show adequate agreement with the surface geology and the gravity in the area. At the Eastern Venezuela Basin a positive velocity anomaly below 30 km depth could indicate the presence of a subducted oceanic slab, as has been postulated to explain the pronounced minimum of the gravity anomaly. In western Venezuela an important low-velocity zone below Moho depth was associated with the triple junction of the Boconó, Oca, and Morón fault systems. Also, low-velocity zones are present below the junction of the Boconó fault zone with the Santa Marta fault zone in southwestern Venezuela and the junction of the La Orchila fault zone with the Boconó-El Pilar fault zone in north-central Venezuela.

Lithospheric seismic velocities below the Moho seem to be related to the major crustal fault systems. Low-velocity zones could be associated with block corners, where multiple junction of different fault systems is taking place. Higher thermal flux at block corners due to local extension might be responsible for the decrease of the compressional velocity. Moderately low velocities are continuous along the major crustal fault systems below 80 km depth.

Acknowledgments. I want to acknowledge Keiiti Aki (Southern California Earthquake Center) and Hakiko Hasemi (Yamagata University) for providing the program VHP used with some modifications to perform the 3-D inversion. Bill Ellsworth (U.S. Geological Survey) kindly provided the program VELEST used after modifications to perform the 1-D inversion. Significant discussion about the geology of eastern Venezuela was held with Mathias Franke (Intevep). Thanks to Albert Tarantola (IPGP) for his reviews of the preliminary version of this manuscript and to Michael Diament (IPGP), who provided a code for gravity modeling. I also acknowledge Michael Hamburguer (JGR-Solid Earth Associate Editor) and two anonymous referees for their valuable comments conducive to the improvement of the manuscript. William Hinze (JGR-Solid Earth Senior Editor) and Michael Hamburguer gently helped to improve the English style and grammar. Graphic facilities were provided by the Universidad Simón Bolivar, Caracas, and computer facilities were provided by the Institut de Physique du Globe de Paris. This research was funded by the Consejo de Desarrollo Científico y Humanístico de la Universidad Central de Venezuela under the identification 09.11.2885.92.

References

Aki, K., and W. H. K. Lee, Determination of the three-dimensional velocity anomalies under a seismic array using P arrival times from local earthquakes, 1, A homogeneous initial model, *J. Geophys. Res., 81*, 4381-4399, 1976.

Bosch, M., and I. Rodríguez, North Venezuelan collisional crustal block: the boundary between the Caribbean and South American plates, *Jour. S. Am. Earth Sci., 6*, 133-143, 1992.

Bosch, M., Inversion 1-D de velocidades de onda-P bajo la red sismologica venezolana, in *Memorias VII Congreso Venezolano de Geofísica*, pp. 22-28, Sociedad Venezolana de Ingenieros Geofísicos (SOVG), Caracas, 1994.

Burov, E. B., and M. Diament, The effective elastic thickness (T_e) of continental lithosphere: What does it really mean?, *J. Geophys. Res., 100*, 3905-3927, 1995.

Case, J. E., W. D. MacDonald, and P. J. Fox, Caribbean crustal provinces: seismic and gravity evidence, in *The Geology of North America*, vol. H,*The Caribbean Region*, edited by G. Dengo and J. E. Case, pp. 15-35, Geol. Soc. of Am., Boulder, Colo., 1990.

Castejón, B., C. Marquez, and M. Urbaez, Modelo de corteza en la Costa Oriental del Lago, engineer thesis, 208 pp., Univ. Cent. de Venezuela, Caracas, 1986.

Censor, Y., Row-action methods for huge and sparse systems and their applications, *Soc. Ind. Appl. Math. Rev., 23*, 444-466, 1981.

Christensen, N. I., Compresional wave velocities in rocks at high temperatures and pressures, critical thermal gradients, and crustal low-velocity zones, *J. Geophys. Res., 84*, 6849-6857, 1979.

Christensen, N. I., and W. D. Mooney, Seismic velocity structure and composition of the continental crust: A global view, *J. Geophys. Res., 100*, 9761-9788, 1995.

DeMets, C., R. G. Gordon, D. F. Argus, and S. Stein, Current plate motions, *Geophys. J. Int., 101*, 425-478, 1990.

Forte, A. M., A. M. Dziewonski, and R. L. Woodward, Aspherical structure of the mantle, tectonic plate motions, nonhydrostatic geoid, and topography of the core-mantle boundary, in *Dynamics of the Earth's Deep Interior and Earth Rotation*, Geophys. Monogr. *Ser.*, vol. 72, edited by J. -L. Mouel, D. E. Smylie, and T. A. Herring, pp. 135-165, AGU, Washington, D. C., 1993.

Franke, M., Seismotektonik und seismische Gefährdung in Nordost-Venezuela abgeleitet von mikroseismischen Messungen, *Ber. Zent. Meeresforsch. Klimaforsch., Reihe C, 3*, 1-99, 1994.

Freymueller, J. T., J. Kellogg, and V. Vega, Plate motions in the North Andean Region, *J. Geophys. Res., 98*, 21,853-21,863, 1993.

Graterol, V., *Mapa de Anomalía de Bouguer* ($P = 2.67 g/cm^3$) *de la República de Venezuela* (1968-1988), Dir. de Cart. Nac., Minis. del Ambiente y los Recursos Nat. Renovables, Caracas, 1988.

Hasemi, A., and M. Ishida, Travel-times and hypocenter determinations by using the three-dimensional velocity model of the Kanto-Tocai District, Japan, *J. Phys. Earth, 35*, 255-271, 1987.

Hirahara, K., A large-scale three-dimensional seismic structure under the Japan Islands and the Sea of Japan, *J. Phys. Earth, 25*, 393-417, 1977.

Hirahara, K., Three-dimensional seismic structure beneath southwest Japan: The subducting Philippine sea plate, *Tectonophysics, 79*, 1-44, 1981.

Hirahara, K., A. Ikami, M. Ishida, and T. Mikumo, Three-dimensional *P* wave velocity structure beneath Central Japan: Low-velocity bodies in the wedge portion of the upper mantle above high-velocity subducting plates, *Tectonophysics, 163*, 63-73, 1989.

Horie, A., Three-dimensional seismic velocity structure beneath the Kanto district by inversion of *P* wave arrival times, Ph.D. thesis, Geophys. Inst. Fac. of Sci., Univ. of Tokyo, 1980.

Horie A., and K. Aki, Three-dimensional velocity structure beneath the Kanto District, Japan, *Journal of Physics of the Earth, 30*, 255-281, 1982.

Huerta, A. D., L. H. Royden, and K. V. Hodges, The interdependence of deformational and thermal processes in mountain belts, *Science, 273*, 637-639, 1996.

Humphreys, E., and R. W. Clayton, Adaptation of back projection tomography to seismic travel time problems, *J. Geophys. Res., 93*, 1073-1085, 1988.

Ishida, M., and A. Hasemi, Three-dimensional fine velocity structure and hypocentral distribution of earthquakes beneath the Kanto-Tokai District, Japan, *J. Geophys. Res., 93*, 2076-2094, 1988.

Jordan, T. H., The present-day motion of the Caribbean plate, *J. Geophys. Res., 80*, 4433-4439, 1975.

Kellogg, J. N., and W. E. Bonini, Subduction of the Caribbean plate and basement uplifts in the overriding South American plate, *Tectonics, 1*, 251-276, 1982.

Kissling, E., W. L. Ellsworth, D. Eberhart-Phillips, and U. Kradolfer, Initial reference models in local earthquake tomography, *J. Geophys. Res., 99*, 19,635-19,646, 1994.

Kumazawa, M., and O. L. Anderson, Elastic moduli, pressure derivatives, and temperature derivatives of single-crystal olivine and single-crystal forsterite, *J. Geophys. Res. , 74*, 5961-5972, 1969.

Ladd, J. W., T. L. Holocombe, G. K. Westbrook, and N. T. Edgar, Caribbean marine geology, Active margins of the plate boundary, in *The Geology of North America*, vol. H, *The Caribbean Region*, edited by G. Dengo and J. E. Case, pp. 261-290, Geol. Soc. of Am., Boulder, Colo., 1990.

Mann, P., C. Schubert, and K. Burke, Review of Caribbean neotectonics, in *The Geology of North America*, Vol H, *The Caribbean Region*, edited by G. Dengo and J. E. Case, pp. 307-338, Geol. Soc. of Am., Boulder, Colo., 1990.

Maquardt, W. D., An algorithm for least-squares estimation of nonlinear parameters, *J. Soc. Ind. App. Math., 11*, 431-441, 1963.

McNutt, M. K., M. Diament, and M. G. Kogan, Variations of elastic plate thickness at continental thrust belts, *J. Geophys. Res., 93*, 8825-8838, 1988.

Mendoza, J., Determinación de un modelo de corteza usando inversion no lineal y tiempos de arribo relativos de eventos sísmicos, in *Memorias 50 Aniversario de la Escuela de Geología, Minas y Geofísica, GEOS, 29*, 300-309, 1989.

Minster, J. B., and T. H. Jordan, Present-day plate motions, *J. Geophys. Res., 83*, 5331-5354, 1978.

Muessig, K. W., Structure and Cenozoic tectonics of the Falcón Basin, Venzuela, and adjacent areas, in *Caribbean-South American Plate Boundary and Regional Tectonics*, edited by W. Bonini, R. Hardgraves, and R. Shagam, *Mem. Geol. Soc. of Am., 162*, 217-230, 1984.

Myers, R., *Classical and Modern Regresion with Applications*, PWS Publ., Boston, Mass., 1986.

Nolet, G., Solving large linearized tomographic problems, in *Seismic Tomography, Theory and Practice*, edited by H. M. Iyer, and K. Hirahara, pp. 227-247, Chapman and Hall, New York, 1993.

Pennington, W. D., Subduction of the eastern Panama Basin and seismotectonics of northwestern South America, *J. Geophys. Res., 86*, 10,753-10,770, 1981.

Pérez, O. J., and Y. P. Aggarwal, Present-day tectonics of the southeastern Caribbean and northeastern Venezuela, *J. Geophys. Res., 86*, 10,791-10,804, 1981.

Pindell, J. L., S. C. Candel, W. C. Pitman, D. B. Rowley, J. Dewey, J. Lebereque, and W. Haxby, A plate-kinematic framework for models of Caribbean evolution, *Tectonophysics, 155*, 121-138, 1988.

Ricard, Y., and C. Vigny, Mantle dynamics with induced plate techtonics, *J. Geophys. Res., 94*, 17,543-17,559, 1989.

Ritzwoller, M. H., and E. L. Lavely, Three-dimensional seismic models of the Earth's mantle, *Rev. Geophys., 33*, 1-66, 1995.

Roecker, S. W., Velocity structure of the Pamir-Hindu Kush Region: Possible evidence of subducted crust, *J. Geophys. Res., 87*, 945-959, 1982.

Ross, M., and C. Scotese, A hierarchical tectonic model of the Gulf of Mexico and Caribbean region, *Tectonophysics, 155*, 139-168, 1988.

Russo, R. M., and R. C. Speed, Oblique collision and tectonic wedging of the South American continent and Caribbean terranes, *Geology, 20*, 447-450, 1992.

Russo, R. M., and R. C. Speed, Spectral analysis of gravity anomalies and the architecture of tectonic wedging, NE Venezuela and Trinidad, *Tectonics, 13*, 613-622, 1994.

Schubert, C., Neotectonics of the Boconó Fault Zone, western Venezuela, *Tectonophysics, 85*, 205-220, 1982.

Schubert, C., Basin formation along the Boconó-Morón-El Pilar fault system, Venezuela, *J. Geophys. Res., 89*, 5711-5718, 1984.

Schubert, C., and F. F. Krause, Morón fault zone, north-central Venezuelan Borderland: Identification, definition and neotectonic character, *Mar. Geophys. Res., 6*, 257-273, 1984.

Silver, E. A., J. E. Case, and H. J. MacGillavry, Geophysical study of the Venezuelan borderland, *Geol. Soc. Am. Bull., 86*, 213-226, 1975.

Speed, R. C., Cenozoic collision of the Lesser Antilles Arc and continental South America and the origin of the El Pilar Fault, *Tectonics, 4*, 41-69, 1985.

Stein, S. S., C. DeMets, R. G. Gordon , J. Bordholt, D. Argus, J. F. Engeln, P. Lundgren, C. Stein, D. A. Wiens, and D. F. Woods, A test of alternative Caribbean plate relative motion models, *J. Geophys. Res., 93*, 3041-3050, 1988.

Thurber, C.H., and W.L. Ellsworth, Rapid solution of ray tracing problems in heterogeneous media, *Bull. Seismol. Soc. Am., 70*, 1137-1148, 1980.

Thurber, G.K., Earthquake locations and three-dimensional crustal structure in the Coyote Lake area, Central California, *J. Geophys. Res., 88*, 8226-8236, 1983.

Van der Hilst, R. D., Tomography with *P*, *PP* and *pP* delay-time data and the three-dimensional mantle structure below the Caribbean region, Ph.D. thesis, 245 pp., Univ. of Utrecht, Netherlands, 1990.

Wiggins, R. A., The general linear inverse problem: Implication of surface waves and free oscilations for earth structure, *Rev. Geophys., 10*, 251-285, 1972.

Woodhouse, J. H., and A. M. Dziewonski, Mapping the upper mantle: Three-dimensional modeling of the Earth structure by inversion of seismic waveforms, *J. Geophys. Res., 89*, 5953-5986, 1984.

Zhao, D. and A. Hasegawa, *P* wave tomographic imaging of the crust and upper mantle beneath the Japan Islands, *J. Geophys. Res., 98*, 4333-4353, 1993.

M. Bosch, Département de Sismologie, Institut de Physique du Globe de Paris, 4 place Jussieu, 75252 Paris Cedex 05, France. (e-mail: bosch@ipgp.jussieu.fr)

(Received February 21, 1996; revised September 25, 1996; accepted October 11, 1996.)